Measurement of the $e^+e^- \to \Lambda\bar{\Sigma}^0 + c.c.$ cross sections at $\sqrt{s}$ from 2.3094 to 3.0800 GeV

M. Ablikim *et al.*[*]
(BESIII Collaboration)

(Received 8 August 2023; revised 27 October 2023; accepted 21 November 2023; published 4 January 2024)

The Born cross sections and effective form factors of the process $e^+e^- \to \Lambda\bar{\Sigma}^0 + \text{c.c.}$ are measured at 14 center-of-mass energy points from 2.3094 to 3.0800 GeV, based on data corresponding to an integrated luminosity of $(478.5 \pm 4.8)\ \text{pb}^{-1}$ collected with the BESIII detector. A nonzero Born cross section is observed at the center-of-mass energy of 2.3094 GeV with a statistical significance of more than five standard deviations, and the cross sections at other energies are obtained with improved precision compared to earlier measurements from the *BABAR* Collaboration. The Born cross-section line shape is described better by a shape considering the strong-interaction effects than by a pQCD motivated functional form.

DOI: 10.1103/PhysRevD.109.012002

I. INTRODUCTION

The electromagnetic form factors (EMFFs) are fundamental observables describing the inner, dynamical structure of hadrons and quantifying their deviation from pointlike particles. Their values can be extracted in space-like and time-like regions via scattering and annihilation processes, respectively. In the timelike region, the EMFFs of baryons have been extensively studied in the pair-production process $e^+e^- \to B\bar{B}$, where B denotes a baryon. For spin $1/2$ baryons, the Born cross section of pair-production can be parametrized in terms of the electric form factor (FF) G_E and the magnetic FF G_M under the one-photon exchange approximation [1],

$$\sigma^B(s) = \frac{4\pi\alpha^2\beta\mathcal{C}\hbar^2c^2}{3s}\left[|G_M(s)|^2 + \frac{1}{2\tau}|G_E(s)|^2\right]. \quad (1)$$

Here, α is the fine-structure constant, $\beta = \sqrt{1-1/\tau}$ is the velocity of the baryon, $\tau = s/4m_B^2c^4$, s is the square of the center-of-mass (c.m.) energy, m_B is the mass of the baryon, and $\mathcal{C}$ is the Coulomb factor, which accounts for the $B\bar{B}$ electromagnetic interactions. The factor $\mathcal{C}$ is unity for neutral baryons, while for charged baryon, $\mathcal{C} = y/(1-e^{-y})$ where $y = \pi\alpha\sqrt{1-\beta^2}/\beta$, resulting in a nonzero cross section at threshold according to Eq. (1). The effective FF $F(s)$ is defined in terms of the moduli squared of G_E and G_M as [2]

$$F(s) \equiv \sqrt{\frac{2\tau|G_M(s)|^2 + |G_E(s)|^2}{2\tau+1}} = \sqrt{\frac{2\tau}{2\tau+1}\frac{3s\sigma^B(s)}{4\pi\alpha^2\beta\mathcal{C}\hbar^2c^2}}. \quad (2)$$

In the past decades, a large number of studies have been performed to investigate the properties of baryons, with many of them relying on the interpretation of the Born cross section of baryon pair-production. Equation (1) indicates that the Born cross section of the $e^+e^- \to B\bar{B}$ process at the production threshold, $\tau = 1$, is nonzero for charged baryon pairs due to the Coulomb correction, and vanishes for neutral baryon pairs. However, the measured cross sections of $e^+e^- \to p\bar{p}$ [3–6] and $e^+e^- \to n\bar{n}$ [7,8] processes both exhibit a flat behavior in the energy range from threshold up to about 2 GeV. Similar behavior near threshold is also observed in the $e^+e^- \to \Lambda\bar{\Lambda}$ process, with the average cross section measured to be 0.3 nb [9–11] and the $e^+e^- \to \Lambda_c^+\bar{\Lambda}_c^-$ process, with the average cross section measured to be 0.2 nb [12]. A similar trend is also observed for the cross sections of $e^+e^- \to \Sigma\bar{\Sigma}$ [13,14] and $e^+e^- \to \Xi\bar{\Xi}$ production [15,16], but larger samples are needed to reach a more reliable conclusion. The plateau near the production threshold in the cross-section line shape seems to be common for a variety of baryon pairs [17]. This abnormal threshold behavior has attracted great interest and stimulated many theoretical explanations, with different hypotheses being proposed such as final-state interactions [18], $B\bar{B}$ bound states, vector meson resonances [19,20], Coulomb final-state interactions or quark electromagnetic interaction and

[*]Full author list given at the end of the article.

the asymmetry between attractive and repulsive Coulomb factors [21,22]. The *BABAR* experiment measured the cross section of the $e^+e^- \to \Lambda\bar{\Sigma}^0 + \mathrm{c.c.}$ (charge conjugate) process via the initial-state radiation (ISR) approach. The cross section in the energy interval from threshold up to 2.400 GeV was found to be $(47^{+23}_{-21} \pm 5)$ pb [11]. Although the uncertainty is large, the result hints at a nonzero cross section at the threshold. This result motivates studying $e^+e^- \to \Lambda\bar{\Sigma}^0 + \mathrm{c.c.}$ production at and above the threshold with improved precision.

In this paper, we present the measurement of the Born cross sections and effective FFs of the $e^+e^- \to \Lambda\bar{\Sigma}^0 + \mathrm{c.c.}$ process at c.m. energies ranging from 2.3094 GeV, which is 1.0 MeV above the $\Lambda\bar{\Sigma}^0$ mass threshold, up to 3.0800 GeV, with the data collected with the BESIII detector at the BEPCII collider. A novel method is applied to measure the Born cross section near threshold and a single-tag technique is used to improve the reconstruction efficiencies at higher energies. In this paper, the charge conjugated process is implied.

II. DETECTOR AND DATA SAMPLE

The BESIII detector [23] records symmetric e^+e^- collisions provided by the BEPCII storage ring [24], which operates in the c.m. energy range from 2.00 to 4.95 GeV. BESIII has collected large data samples in this energy region [25]. The cylindrical core of the BESIII detector covers 93% of the full solid angle and consists of a helium-based multilayer drift chamber (MDC), a plastic scintillator time-of-flight system (TOF), and a CsI(Tl) electromagnetic calorimeter (EMC), which are all enclosed in a superconducting solenoidal magnet providing a 1.0 T magnetic field [26]. The solenoid is supported by an octagonal flux-return yoke with resistive plate counter muon-identification modules interleaved with steel. The charged-particle momentum resolution at 1 GeV/c is 0.5%, and the $\mathrm{d}E/\mathrm{d}x$ resolution is 6% for electrons from Bhabha scattering. The EMC measures photon energies with a resolution of 2.5% (5%) at 1 GeV in the barrel (end caps) region. The time resolution in the TOF barrel region is 68 ps, while that in the end-cap region is 110 ps.

Simulated data samples produced with a Geant4-based [27] Monte Carlo (MC) package, which includes the geometric and material description of the BESIII detector and the detector response, are used to determine detection efficiencies and estimate background. The simulation models the beam-energy spread and initial-state radiation (ISR) in the e^+e^- annihilations with the generator CONEXC [28]. All particle decays are modeled with EvtGen [29,30] using branching fractions taken from the Particle Data Group (PDG) [31]. Final-state radiation from charged final-state particles is incorporated with the PHOTOS [32] package.

The $\Lambda/\bar{\Lambda}$ and $\Sigma^0/\bar{\Sigma}^0$ in the signal channel of $e^+e^- \to \Lambda\bar{\Sigma}^0$, and dominant background channels of $e^+e^- \to \Lambda\bar{\Lambda}$ and $e^+e^- \to \Sigma^0\bar{\Sigma}^0$ are simulated in the $\Lambda \to p\pi^-/\bar{\Lambda} \to \bar{p}\pi^+$ and $\Sigma^0 \to \gamma\Lambda/\bar{\Sigma}^0 \to \gamma\bar{\Lambda}$ decay modes.

III. RECONSTRUCTION OF $e^+e^- \to \Lambda\bar{\Sigma}^0$ AT $\sqrt{s} = 2.3094$ GeV

The $e^+e^- \to \Lambda\bar{\Sigma}^0$ process is expected to dominantly produce the final state $\gamma p\bar{p}\pi^+\pi^-$ at $\sqrt{s} = 2.3094$ GeV, which is only 1 MeV above the kinematic threshold. Furthermore, the decay products of $\Lambda \to p\pi^-$ decays are close to its threshold, as are those of $\bar{\Sigma}^0$ decays. Therefore, the particles in the final state $\gamma p\bar{p}\pi^+\pi^-$ have low momenta and are unlikely to all be reconstructed by the BESIII detector. However, low-momentum antiprotons can interact with the material in the detector, mostly the beam pipe, and produce secondary particles which is reconstructable. Moreover, the low momenta pions from the signal process are quasimonoenergetic. Instead of requiring that all final-state particles $\gamma p\bar{p}\pi^+\pi^-$ are reconstructed, an indirect search for the secondary product from the antiproton interaction and the monoenergetic pions is employed. Similar method has been also used in Refs. [9,14].

Charged tracks detected in the MDC are required to be within $|\cos\theta| < 0.93$, where θ is defined with respect to the z-axis, which is the symmetry axis of the MDC. The distance of closest approach to the interaction point (IP) must be less than 10 cm along the z-axis and less than 1 cm in the transverse plane.

Particle identification (PID) for charged tracks combines measurements of the specific ionization energy loss in the MDC ($\mathrm{d}E/\mathrm{d}x$) and the time of flight in the TOF to calculate a likelihood $\mathcal{L}(h)(h = p, K, \pi, e)$ for each h hypothesis. Tracks are identified as pions when the pion hypothesis has the highest likelihood value $\mathcal{L}(\pi) > \mathcal{L}(p, K, e)$. Events with only one π^+ and one π^- reconstructed are kept for further analysis. Considering the low momenta of the Λ and $\bar{\Sigma}^0$, and the vertex resolution, the π tracks are assumed to arise from the same vertex. A vertex fit [33] is applied to the two π tracks and the transverse distance of the vertex with respect to the beam is required to be less than 2 cm. Both the momenta of the π^+ and π^- tracks in the laboratory frame peak at around 0.1 GeV/c. The momentum of the π^- track is required to lie in the range $(0.08, 0.12)$ GeV/c to suppress background, and the momentum of π^+ track is used to fit the signal contribution.

The low-momentum antiprotons from the signal decay predominantly interact with the material in the detector, specifically the beam pipe, resulting in the production of the secondary particles. To identify antiprotons, at least two additional charged tracks are required to originate from a common vertex. Since the source of these secondaries are expected to be dominated by annihilations in the beam pipe whose inner radius is 3.15 cm and outer radius is 3.37 cm, the transverse distance of their vertex with respect to the beam must lie between 1 and 5 cm.

Two sources of contamination are investigated: physical and beam-associated background. The physical background is studied with inclusive MC samples and the beam-associated background is studied with special separated-beam data taken at $\sqrt{s} = 2.2324$ and 2.6444 GeV, where the centers of e^+ and e^- beam bunch are separated and do not collide at the IP, but the dataset is not sufficient enough to extract the background shape for fitting. Therefore, a data sample taken at $\sqrt{s} = 2.1250$ GeV, which is below the production threshold for the signal process, is also used to study the beam-associated background and the physical background other than the $\Lambda\bar{\Lambda}$ process.

The number of signal events is extracted by an unbinned maximum-likelihood fit to the momentum distribution of the π^+ tracks. A signal yield of 49.9 ± 8.6 events with a statistical significance of 7.7 standard deviations is obtained by comparing the change in the log likelihood between the fits with and without the signal component, as shown in Fig. 1. The signal is described with an MC shape convolved with a Gaussian function describing momentum-resolution difference between data and MC simulation. The background from the $e^+e^- \to \Lambda\bar{\Lambda}$ process is described by the MC shape. The other physical background and beam-associated background are described by the shape extracted from the data taken at $\sqrt{s} = 2.1250$ GeV, which has the highest integrated luminosity below the threshold of the signal process. The numbers of both background events are free in the fit.

The Born cross section of the $e^+e^- \to \Lambda\bar{\Sigma}^0$ process is calculated by

$$\sigma^B(s) = \frac{N_{\rm obs}}{\mathcal{L} \cdot \epsilon \cdot (1+\delta) \cdot \mathcal{B}}, \tag{3}$$

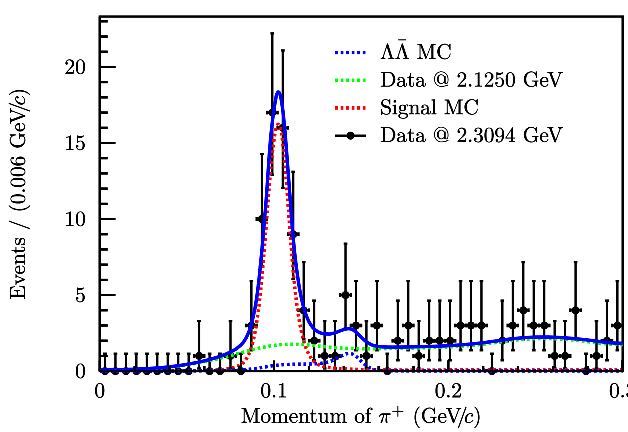

FIG. 1. Fitted momentum distribution of reconstructed π^+ tracks in the laboratory frame, showing the contributions of the signal together with the background from $e^+e^- \to \Lambda\bar{\Lambda}$ events as determined from MC simulation and the other background determined from data at 2.1250 GeV.

TABLE I. Relative systematic uncertainties on the Born cross section measurement at $\sqrt{s} = 2.3094$ GeV.

Source	Uncertainty (%)
Luminosity	1.0
$\pi^\pm$ tracking	4.6
$\pi^\pm$ PID	2.0
Branching fraction	1.6
MC sample size	0.8
$\bar{p}$ annihilation	2.4
Signal shape	2.4
Background shape	2.5
Energy spread	2.7
$1+\delta$ calculation	0.5
Total	7.4

where $N_{\rm obs}$ is the number of observed signal events in data, $\mathcal{L}$ is the integrated luminosity, ϵ is the detection efficiency, $1+\delta$ is the radiative correction factor due to the ISR and the vacuum polarization. Both ϵ and $1+\delta$ are determined from MC simulation. $\mathcal{B}$ is the product of the branching fractions of $\Lambda \to p\pi^-$, $\bar{\Sigma}^0 \to \gamma\bar{\Lambda}$ and $\bar{\Lambda} \to \bar{p}\pi^+$.

Several sources of systematic uncertainties are considered in the Born cross-section measurement at $\sqrt{s} = 2.3094$ GeV, which are summarized in Table I. The integrated luminosity is measured with 1.0% precision [34,35]. The uncertainties from $\pi^\pm$ tracking and PID efficiencies are determined from a control sample of $J/\psi \to p\bar{p}\pi^+\pi^-$ decays by focusing on $\pi^\pm$ with momentum overlapped with the signal process, and estimated as 4.6% and 2.0%, respectively. The uncertainty of $\mathcal{B}(\Lambda \to p\pi^-)$ is 0.8% [31]. The uncertainty associated with the limited size of the signal MC sample is calculated as $\frac{1}{\sqrt{N_{\rm gen}}} \cdot \sqrt{\frac{1-\epsilon}{\epsilon}}$, where $N_{\rm gen}$ is the number of events generated in simulation. The uncertainties introduced by selection criteria, including the requirement on the π^- momentum and the transverse distance of the vertex, are studied by varying the criteria and found to be negligible. The uncertainty from the ISR process is found to be dominated by the accuracy of $1+\delta$ calculation in the CONEXC generator and quoted as 0.5% [28]. The uncertainty associated with the $\bar{p}$ annihilation in the beam pipe is studied from a control sample of $J/\psi \to p\bar{p}\pi^+\pi^-$ events by focusing on $\bar{p}$ with momentum overlapped with the signal process, and is determined to be 2.4%.

The uncertainty associated with the choice of signal shape is estimated by changing the signal shape to a pure MC shape without the convolved Gaussian function. The uncertainty associated with the background shape is estimated by replacing the shape with one extracted at $\sqrt{s} = 2.0000$ and 2.1000 GeV. The difference in the signal yields is taken as the uncertainty. To study the uncertainty from the c.m. energy spread, a new signal MC sample

TABLE II. The luminosity ($\mathcal{L}$), signal yield ($N_{\rm obs}$), detection efficiency (ϵ), radiative correction factor $(1+\delta)$ and obtained Born cross section ($\sigma^{\rm B}$) for the $e^+e^- \to \Lambda\bar{\Sigma}^0$ process at 2.3094 GeV. For the numerical result of the cross section, the first uncertainty is statistical and the second one is systematic. The uncertainty for the signal yields is statistical only.

$\mathcal{L}$ (pb^{-1})	21.1
$N_{\rm obs}$	49.9 ± 8.6
ϵ	0.127
$1+\delta$	0.627
$\sigma^{\rm B}$ (pb)	$72.9 \pm 12.6 \pm 5.4$

including the energy spread is generated, and the difference in $\epsilon \cdot (1+\delta)$ is taken as the uncertainty. All the systematic uncertainties are considered uncorrelated and summed in quadrature as listed in Table I. And the resulting Born cross section is summarized in Table II.

IV. RECONSTRUCTION OF $e^+e^- \to \Lambda\bar{\Sigma}^0$ AT HIGHER ENERGIES

At c.m. energies from $\sqrt{s} = 2.3864$ to 3.0800 GeV, the final-state particles have enough momentum to be reconstructed, but the full reconstruction still suffers from low efficiency. Hence, a single Λ-tag technique is employed, i.e., only the Λ from the primary interaction is reconstructed via the decay $\Lambda \to p\pi^-$, and the presence of the $\bar{\Sigma}^0$ is inferred from the recoil mass.

Charged tracks are reconstructed with the same method described in Sec. III, except that the distance of closest approach to the IP must be less than 30 cm along the beam direction and less than 10 cm in the transverse plane. A charged track is identified as a pion (proton) when the pion (proton) hypothesis has the highest likelihood value $\mathcal{L}(\pi) > \mathcal{L}(p,K)$ [$\mathcal{L}(p) > \mathcal{L}(\pi,K)$]. Events with only one $p\pi^-$ pair are kept for further analysis.

A primary-vertex fit [33] is preformed based on the $p\pi^-$ track information to find the decay vertex of the Λ candidate. And a secondary-vertex fit [36] is then performed based on the interaction point of e^+e^- and decay vertex of the Λ candidate to extract the decay length of the Λ candidate, which is the distance between the production vertex and decay vertex of the Λ candidate. The decay length is required to be greater than twice of its resolution. The sum of χ^2 values of primary vertex fit and secondary vertex fit is required to be less than 50. The invariant mass of the $p\pi^-$ combination is required to be within $[1.11, 1.12]$ GeV/c^2.

The $\bar{\Sigma}^0$ candidate is inferred from the invariant mass of the system recoiling against the selected Λ candidate

$$M^{\rm recoil}_{p\pi} = \sqrt{\frac{E^2_{\bar{\Sigma}^0}}{c^4} - \frac{|\vec{p}_{p\pi^-}|^2}{c^2}},$$

where $E_{\bar{\Sigma}^0}$ is the expected energy of the $\bar{\Sigma}^0$, i.e., $E_{\bar{\Sigma}^0} = (s + m^2_{\bar{\Sigma}^0}c^4 - m^2_\Lambda c^4)/2\sqrt{s}$, and m_Λ and $m_{\bar{\Sigma}^0}$ are the known masses of the labeled baryons from the PDG [31]. Here $\vec{p}_{p\pi^-}$ is the three-momenta of the Λ candidate.

Potential sources of background are investigated by studying the inclusive hadronic MC samples. The dominant background processes are $e^+e^- \to \Lambda\bar{\Lambda}$ and $e^+e^- \to \Sigma^0\bar{\Sigma}^0$ with final states of $p\bar{p}\pi^+\pi^-$ and $\gamma\gamma p\bar{p}\pi^+\pi^-$, respectively. In addition, the Λ produced by the decay of the Σ^0 in the $e^+e^- \to \bar{\Lambda}\Sigma^0$ process also contributes to the background. Besides background from Λ recoil, there is also combinatorial background which can be estimated using the Λ sidebands. The Λ sidebands defined as $M_{p\pi} \in (1.095, 1.105)$ GeV/c^2 and $M_{p\pi} \in (1.125, 1.135)$ GeV/c^2 are inspected, and indicate that there is a nonzero level of combinatorial background, but no significant peaking contamination.

The $e^+e^- \to \Lambda\bar{\Sigma}^0$ signal yields at each energy point are extracted by an unbinned maximum-likelihood fit to the $M^{\rm recoil}_{p\pi}$ spectrum, an example of which is shown at $\sqrt{s} = 2.6444$ GeV in Fig. 2. The signal is described with the shape obtained from MC, convolved with a Gaussian function to compensate for possible mass-resolution difference between data and MC simulation. The background is modeled with the MC shapes of the $e^+e^- \to \Lambda\bar{\Lambda}$ process, the $e^+e^- \to \Sigma^0\bar{\Sigma}^0$ process, the Λ from Σ^0 decay in the signal process and the sideband shape from experimental data. The MC shape of the $e^+e^- \to \Lambda\bar{\Lambda}$ process is convolved with the same Gaussian function as the signal shape. The MC shape of Λ from Σ^0 in the $e^+e^- \to \bar{\Lambda}\Sigma^0$ process is fixed according to the signal MC sample. The Born cross

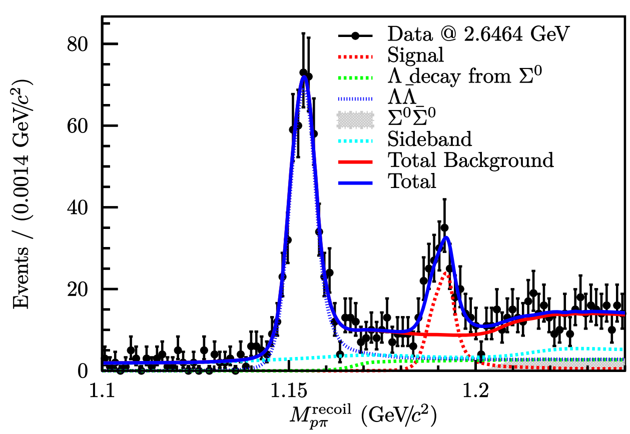

FIG. 2. Fitted distribution of $M^{\rm recoil}_{p\pi}$ at $\sqrt{s} = 2.6464$ GeV. The black dots with error bars are the data, The blue solid line is the fit result, and the red solid line is the overall background. The red dashed line represents the signal, the blue dashed line represents the $\Lambda\bar{\Lambda}$ background, the green dashed line represents the background where Λ decays from Σ^0, the cyan dashed line represents the background extracted from $M_{p\pi}$ sideband, and the gray filled curve represents the $\Sigma^0\bar{\Sigma}^0$ background.

TABLE III. Relative systematic uncertainties (in %) in the cross section measurement for each c.m. energy ($\sqrt{s}$) above 2.3864 GeV: the uncertainty associated with luminosity ($\mathcal{L}$), Λ reconstruction (Λ), MC sample size (ϵ), branching fraction ($\mathcal{B}$), Λ angular distribution (Angle), signal shape, sideband shape (Sideband), $\Lambda\bar{\Lambda}$ background shape ($\Lambda\bar{\Lambda}$ shape), $\Sigma^0\bar{\Sigma}^0$ background shape ($\Sigma^0\bar{\Sigma}^0$ shape), signal input line shape and $1+\delta$ calculation ($1+\delta$). The last column gives the total systematic uncertainty.

$\sqrt{s}$ (GeV)	$\mathcal{L}$	Λ	ϵ	$\mathcal{B}$	Angle	Signal shape	Sideband	$\Lambda\bar{\Lambda}$ shape	$\Sigma\bar{\Sigma}^0$ shape	$1+\delta$	Total
2.3864	1.0	2.6	0.9	0.8	7.8	1.7	7.7	0.9	0.0	0.5	11.5
2.3960	1.0	2.6	0.8	0.8	7.4	1.3	1.1	0.5	0.0	0.5	8.2
2.5000	1.0	2.6	0.5	0.8	6.7	2.5	2.5	3.7	2.3	0.5	9.3
2.6444	1.0	3.3	0.4	0.8	5.7	0.7	3.5	7.9	0.1	0.5	10.9
2.6464	1.0	3.3	0.4	0.8	6.1	0.3	6.8	8.3	0.6	0.5	12.9
2.7000	1.0	3.3	0.4	0.8	5.7	0.3	6.8	8.3	0.6	0.5	12.7
2.8000	1.0	3.3	0.4	0.8	5.6	2.6	5.5	7.3	4.6	0.5	12.5
2.9000	1.0	3.3	0.5	0.8	5.4	0.6	2.9	0.9	1.5	0.5	7.3
2.9500	1.0	3.1	0.5	0.8	5.8	0.4	13.8	0.5	0.3	0.5	15.3
2.9810	1.0	3.1	0.5	0.8	5.7	0.2	0.1	2.2	10.2	0.5	12.4
3.0000	1.0	3.1	0.5	0.8	5.8	0.1	3.3	1.6	1.4	0.5	7.8
3.0200	1.0	3.1	0.5	0.8	5.9	3.2	3.9	1.7	2.9	0.5	9.1
3.0800	1.0	3.1	0.5	0.8	5.7	0.5	4.0	2.6	4.4	0.5	9.3

section is determined using Eq. (3), where $\mathcal{B}$ is the branching fraction of the decay $\Lambda \to p\pi^-$.

Various sources of systematic uncertainties have been considered in Born cross-section measurements in this energy regime, with a summary presented in Table III. The uncertainties associated with the luminosity measurement, branching fraction knowledge, MC sample size, signal line shape and $1+\delta$ calculation are assigned following the same procedure as described in the previous section. The uncertainty associated with the reconstruction of the Λ is determined from the control samples $J/\psi \to \bar{p}K^+\Lambda$ and $J/\psi \to \Lambda\bar{\Lambda}$, with a similar method as used in Ref. [37]. To estimate the uncertainty coming from the knowledge of the angular distribution of the Λ baryon, the analysis is repeated with the two extremes of the angular distributions $(1+\cos^2\theta)$ and $(1-\cos^2\theta)$ [38]. The difference in the resulting efficiencies divided by $\sqrt{12}$ is taken as the uncertainty. Alternative fits are performed to study the uncertainties associated with the fit shapes. These include changing the default signal shape to a pure MC shape without the convolved Gaussian function, varying the regions of sideband background to only $[1.095, 1.105]$ GeV$/c^2$ or $[1.125, 1.135]$ GeV$/c^2$, replacing the input line shape of $\Lambda\bar{\Lambda}$ background MC sample with one extracted from the cross section of the Λ pair production at BESIII experiment [9,10] instead of the fitted result from *BABAR* experiment [11], and fixing the background shape of the $\Sigma^0\bar{\Sigma}^0$ process according to the integrated luminosity and its cross section. Any potential bias arising from the requirement on the χ^2 of the vertex fit is investigated by varying the boundaries from 20 to 100, and that from the mass-window requirement of the Λ candidate is estimated by varying the left boundary from 1.109 to 1.112 GeV$/c^2$ and the right boundary from 1.118 to 1.122 GeV$/c^2$. Both of these contributions are found to be negligible, and no uncertainties are assigned. All the systematic uncertainties are considered uncorrelated and summed in quadrature.

V. RESULTS AND CONCLUSION

For the $e^+e^- \to \Lambda\bar{\Sigma}^0$ process, the expressions of Eqs. (1) and (2) need to be modified by the substitutions [11,39],

$$\beta = \sqrt{1 - \frac{2(m_{\bar{\Sigma}^0}^2 + m_\Lambda^2)c^4}{s} + \frac{(m_{\bar{\Sigma}^0}^2 - m_\Lambda^2)^2 c^8}{s^2}}, \quad (4)$$

$$\tau = \frac{s}{(m_\Lambda + m_{\bar{\Sigma}^0})^2 c^4}. \quad (5)$$

The resulting Born cross sections and the effective FFs are summarized in Table IV, and a comparison between the results of this work and those of *BABAR* is illustrated in Fig. 3.

A perturbative QCD (pQCD) motivated energy power function [40], given by

$$\sigma^{\mathrm{B}}(s) = \frac{c_0 \cdot \beta \cdot \mathcal{C}}{(\sqrt{s} - c_1)^{10}}, \quad (6)$$

is used to fit the line shape, where c_0 and c_1 are free parameters and the Coulomb correction factor $\mathcal{C}$ is 1 for a neutral channel. Figure 3(a) shows the fit result, with $c_0 = (9.94 \pm 3.91) \times 10^3$ pb GeV^{10}, $c_1 = (0.97 \pm 0.07)$ GeV and fit quality $\chi^2/ndof = 41.0/12 = 3.42$, where $ndof$ is the number of degrees of freedom. From the fit quality, the nonzero cross section at threshold does not fit to the pQCD model.

Inspired by the nucleon pair-production cross section and its plateau near threshold region [6], another empirical

TABLE IV. The luminosity ($\mathcal{L}$), signal yield (N_{obs}), detection efficiency (ϵ), radiative correction factor ($1+\delta$), obtained Born cross section (σ^{B}) and effective FF [$F(s)$] for the $e^+e^- \to \Lambda\bar{\Sigma}^0$ process at each c.m. energy ($\sqrt{s}$). The first uncertainties are statistical and the second ones are systematic. The uncertainties for the signal yields are statistical only.

$\sqrt{s}$ (GeV)	$\mathcal{L}$ (pb^{-1})	N_{obs}	ϵ	$1+\delta$	σ^{B} (pb)	$F(s)$
2.3094	21.1	49.9 ± 8.6	0.127	0.627	$72.9 \pm 12.6 \pm 5.4$	$0.312 \pm 0.027 \pm 0.012$
2.3864	22.5	124.2 ± 11.8	0.107	0.886	$91.4 \pm 8.7 \pm 10.6$	$0.127 \pm 0.006 \pm 0.007$
2.3960	66.9	447.2 ± 22.1	0.134	0.896	$87.3 \pm 4.3 \pm 7.1$	$0.121 \pm 0.003 \pm 0.005$
2.5000	1.10	7.6 ± 2.8	0.301	0.985	$36.6 \pm 13.3 \pm 3.4$	$0.069 \pm 0.013 \pm 0.003$
2.6444	33.7	183.8 ± 16.0	0.338	1.095	$23.1 \pm 2.0 \pm 2.5$	$0.053 \pm 0.002 \pm 0.003$
2.6464	34.0	163.2 ± 15.4	0.338	1.096	$20.3 \pm 1.9 \pm 2.6$	$0.049 \pm 0.002 \pm 0.003$
2.7000	1.03	0.0 ± 2.3	0.344	1.140	$0.0 \pm 8.9 \pm 0.0$	$0.000 \pm 0.033 \pm 0.000$
2.8000	1.01	1.8 ± 1.6	0.333	1.231	$6.8 \pm 6.0 \pm 0.9$	$0.029 \pm 0.012 \pm 0.002$
2.9000	106	272.0 ± 18.8	0.312	1.337	$9.6 \pm 0.7 \pm 0.7$	$0.034 \pm 0.001 \pm 0.001$
2.9500	15.9	25.9 ± 7.1	0.295	1.397	$6.2 \pm 1.7 \pm 0.9$	$0.028 \pm 0.004 \pm 0.002$
2.9810	16.1	30.9 ± 6.1	0.297	1.436	$7.0 \pm 1.4 \pm 0.9$	$0.030 \pm 0.003 \pm 0.002$
3.0000	15.9	30.6 ± 6.3	0.289	1.461	$7.1 \pm 1.5 \pm 0.6$	$0.030 \pm 0.003 \pm 0.001$
3.0200	17.3	27.3 ± 5.9	0.287	1.486	$5.8 \pm 1.2 \pm 0.5$	$0.027 \pm 0.003 \pm 0.001$
3.0800	126	136.9 ± 14.4	0.254	1.511	$4.4 \pm 0.5 \pm 0.4$	$0.024 \pm 0.001 \pm 0.001$

prediction of the Born cross section is used to describe the line shape, which takes into account strong-interaction effects near the threshold,

$$\sigma^{\mathrm{B}}(s) = \frac{e^{a_0}\pi^2\alpha^3\hbar^2c^2}{s\left[1-e^{-\frac{\pi\alpha_s(s)}{\beta(s)}}\right]\left[1+\left(\frac{\sqrt{s}-(m_\Lambda+m_{\bar{\Sigma}^0})c^2}{a_1}\right)^{a_2}\right]}. \quad (7)$$

Here a_0, a_1, a_2 are free parameters, a_0 is the normalization constant, a_1 is the QCD parameter near threshold, a_2 is a power-law parameter related to the number of valence quarks, α is the electromagnetic coupling constant and $\alpha_s(s)$ is the strong running coupling constant,

$$\alpha_s(s) = \left[\frac{1}{\alpha_s(m_Z^2c^4)} + \frac{25}{12\pi}\ln\left(\frac{s}{m_Z^2c^4}\right)\right]^{-1}, \quad (8)$$

where $m_Z = 91.1876$ GeV$/c^2$ is the Z boson mass and $\alpha_s(m_Z^2c^4) = 0.11856$. Figure 3(a) also shows the fit result, with $a_0 = -1.09 \pm 0.10$, $a_1 = (0.20 \pm 0.03)$ GeV, $a_2 = 2.00 \pm 0.17$ and $\chi^2/ndof = 13.7/11 = 1.25$. The description of Eq. (7) that includes strong-interaction effects gives a better fit quality than the pQCD prediction. Figure 3(b) shows the effective FFs obtained in this work and previous measurement at *BABAR*. Except for the c.m. energy of 2.3094 GeV, our measured results are consistent with earlier results from *BABAR*, with improved precision.

VI. SUMMARY

Based on a total integrated luminosity of 478.5 pb^{-1} e^+e^- collision data collected with the BESIII detector, the Born cross sections and effective form factors of the $e^+e^- \to \Lambda\bar{\Sigma}^0$ process have been determined at c.m. energies ranging from 2.3094 up to 3.0800 GeV. At $\sqrt{s} =$ 2.3094 GeV, which is approximately 1 MeV above the threshold, the signal process is identified by the primary pion from the signal decay and secondary tracks from the interaction of antiproton with beam pipe. A nonzero

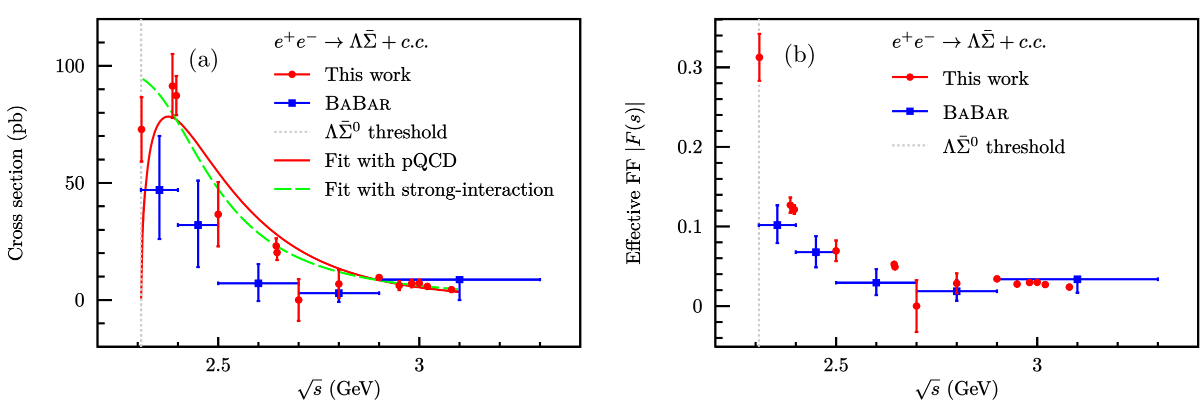

FIG. 3. (a) The Born cross sections and (b) effective FFs for the $e^+e^- \to \Lambda\bar{\Sigma}^0$ + c.c. process from this analysis shown with fits to the pQCD model [Eq. (6)] and a model with strong-interaction effects included [Eq. (7)]. Also shown are the results obtained by *BABAR*.

Born cross section is found with a statistical significance greater than 5 standard deviations and measured to be $(72.9 \pm 12.6 \pm 5.4)$ pb, where the first uncertainty is statistical and the second is systematic. At other energies, a single-tag technique is employed by tagging the primary Λ alone to optimize the detection efficiency. The Born cross sections at these energies are in good agreement with those of *BABAR*, but with improved precision. Fits with pQCD assumption and strong-interaction effects are performed on the line shape of the Born cross sections, and it is found that the latter gives a better description of the data. The measured effective FFs are consistent with *BABAR*'s results for the c.m. energies above 2.3094 GeV.

ACKNOWLEDGMENTS

The BESIII Collaboration thanks the staff of BEPCII and the IHEP computing center and the supercomputing center of USTC for their strong support. This work is supported in part by National Key R&D Program of China under Contracts No. 2020YFA0406400, No. 2020YFA0406300; National Natural Science Foundation of China (NSFC) under Contracts No. 12105276, No. 11625523, No. 12035013, No. 12061131003, No. 12122509, No. 11635010, No. 11735014, No. 11835012, No. 11935015, No. 11935016, No. 11935018, No. 11961141012, No. 12022510, No. 12025502, No. 12035009, No. 12192260, No. 12192261, No. 12192262, No. 12192263, No. 12192264, No. 12192265, No. 12221005, No. 12235017; Joint Large-Scale Scientific Facility Funds of the NSFC and CAS under Contracts No. U1732263, No. U1832103, No. U2032111; Knut and Alice Wallenberg Foundation under Contracts No. 2016.0157 and No. 2021.0299; Swedish Research Council under Contracts No. 2019-04594 and No. 2021-04567; Swedish Foundation for International Cooperation in Research and Higher Education under Contract No. CH2018-7756; Olle Engkvist Foundation under Contract No. 200-0605; Lundström-Åman Foundation; the Chinese Academy of Sciences (CAS) Large-Scale Scientific Facility Program; the CAS Center for Excellence in Particle Physics (CCEPP); CAS Key Research Program of Frontier Sciences under Contracts No. QYZDJ-SSW-SLH003, No. QYZDJ-SSW-SLH040; 100 Talents Program of CAS; The Institute of Nuclear and Particle Physics (INPAC) and Shanghai Key Laboratory for Particle Physics and Cosmology; ERC under Contract No. 758462; European Union's Horizon 2020 research and innovation programme under Marie Sklodowska-Curie grant agreement under Contract No. 894790; German Research Foundation DFG under Contracts No. 443159800, No. 455635585, Collaborative Research Center CRC 1044, FOR5327, GRK 2149; Istituto Nazionale di Fisica Nucleare, Italy; Ministry of Development of Turkey under Contract No. DPT2006K-120470; National Research Foundation of Korea under Contract No. NRF-2022R1A2C1092335; National Science and Technology fund of Mongolia; National Science Research and Innovation Fund (NSRF) via the Program Management Unit for Human Resources & Institutional Development, Research and Innovation of Thailand under Contract No. B16F640076; Polish National Science Centre under Contract No. 2019/35/O/ST2/02907; The Swedish Research Council; U.S. Department of Energy under Contract No. DE-FG02-05ER41374.

[1] N. Cabibbo and R. Gatto, Phys. Rev. **124**, 1577 (1961).
[2] M. Bertani, A. Mangoni, and S. Pacetti, Symmetry **14**, 439 (2022).
[3] B. Aubert *et al.* (*BABAR* Collaboration), Phys. Rev. D **73**, 012005 (2006).
[4] J. P. Lees *et al.* (*BABAR* Collaboration), Phys. Rev. D **87**, 092005 (2013).
[5] M. Ablikim *et al.* (BESIII Collaboration), Phys. Rev. D **91**, 112004 (2015).
[6] M. Ablikim *et al.* (BESIII Collaboration), Phys. Rev. Lett. **124**, 042001 (2020).
[7] M. N. Achasov *et al.* (SND Collaboration), Phys. Rev. D **90**, 112007 (2014).
[8] M. Ablikim *et al.* (BESIII Collaboration), Nat. Phys. **17**, 1200 (2021).
[9] M. Ablikim *et al.* (BESIII Collaboration), Phys. Rev. D **97**, 032013 (2018).
[10] M. Ablikim *et al.* (BESIII Collaboration), Phys. Rev. Lett. **123**, 122003 (2019).
[11] B. Aubert *et al.* (*BABAR* Collaboration), Phys. Rev. D **76**, 092006 (2007).
[12] M. Ablikim *et al.* (BESIII Collaboration), Phys. Rev. Lett. **120**, 132001 (2018).
[13] M. Ablikim *et al.* (BESIII Collaboration), Phys. Lett. B **814**, 136110 (2021).
[14] M. Ablikim *et al.* (BESIII Collaboration), Phys. Lett. B **831**, 137187 (2022).
[15] M. Ablikim *et al.* (BESIII Collaboration), Phys. Rev. D **103**, 012005 (2021).
[16] M. Ablikim *et al.* (BESIII Collaboration), Phys. Lett. B **820**, 136557 (2021).
[17] G. S. Huang and R. Baldini Ferroli, Natl. Sci. Rev. **8**, nwab187 (2021).

[18] J. Haidenbauer, U.-G. Meißner, and L. Y. Dai, Phys. Rev. D **103**, 014028 (2021).
[19] O. D. Dalkarov, P. A. Khakhulin, and A. Y. Voronin, Nucl. Phys. **A833**, 104 (2010).
[20] B. El-Bennich, M. Lacombe, B. Loiseau, and S. Wycech, Phys. Rev. C **79**, 054001 (2009).
[21] R. Baldini, S. Pacetti, A. Zallo, and A. Zichichi, Eur. Phys. J. A **39**, 315 (2009).
[22] R. Baldini Ferroli, S. Pacetti, and A. Zallo, Eur. Phys. J. A **48**, 33 (2012).
[23] M. Ablikim *et al.* (BESIII Collaboration), Nucl. Instrum. Methods Phys. Res., Sect. A **614**, 345 (2010).
[24] C. H. Yu *et al.*, in *Proceedings of the 7th International Particle Accelerator Conference* (JACoW, Busan, Korea, 2016), p. TUYA01, 10.18429/JACoW-IPAC2016-TUYA01.
[25] M. Ablikim *et al.* (BESIII Collaboration), Chin. Phys. C **44**, 040001 (2020).
[26] K. X. Huang *et al.*, Nucl. Sci. Tech. **33**, 142 (2022).
[27] S. Agostinelli *et al.* (Geant4 Collaboration), Nucl. Instrum. Methods Phys. Res., Sect. A **506**, 250 (2003).
[28] R. G. Ping, Chin. Phys. C **38**, 083001 (2014).
[29] D. J. Lange, Nucl. Instrum. Methods Phys. Res., Sect. A **462**, 152 (2001).
[30] R. G. Ping, Chin. Phys. C **32**, 599 (2008).
[31] R. L. Workman and Others (Particle Data Group), Prog. Theor. Exp. Phys. **2022**, 083C01 (2022).
[32] E. Richter-Was, Phys. Lett. B **303**, 163 (1993).
[33] M. Xu *et al.*, Chin. Phys. C **34**, 92 (2010).
[34] M. Ablikim *et al.* (BESIII Collaboration), Chin. Phys. C **41**, 063001 (2017).
[35] M. Ablikim *et al.* (BESIII Collaboration), Chin. Phys. C **41**, 113001 (2017).
[36] M. Xu *et al.*, Chin. Phys. C **33**, 428 (2009).
[37] M. Ablikim *et al.* (BESIII Collaboration), Phys. Rev. Lett. **121**, 062003 (2018).
[38] R. Wanke, *Data Analysis in High Energy Physics* (Wiley-VCH Verlag GmbH and Co. KGaA, 2013), pp. 263–280, 10.1002/9783527653416.ch8.
[39] R. Baldini Ferroli, A. Mangoni, S. Pacetti, and K. Zhu, Phys. Lett. B **799**, 135041 (2019).
[40] S. Pacetti, R. Baldini Ferroli, and E. Tomasi-Gustafsson, Phys. Rep. **550–551**, 1 (2015).

M. Ablikim,[1] M. N. Achasov,[13,b] P. Adlarson,[75] X. C. Ai,[81] R. Aliberti,[36] A. Amoroso,[74a,74c] M. R. An,[40] Q. An,[71,58] Y. Bai,[57] O. Bakina,[37] I. Balossino,[30a] Y. Ban,[47,g] V. Batozskaya,[1,45] K. Begzsuren,[33] N. Berger,[36] M. Berlowski,[45] M. Bertani,[29a] D. Bettoni,[30a] F. Bianchi,[74a,74c] E. Bianco,[74a,74c] J. Bloms,[68] A. Bortone,[74a,74c] I. Boyko,[37] R. A. Briere,[5] A. Brueggemann,[68] H. Cai,[76] X. Cai,[1,58] A. Calcaterra,[29a] G. F. Cao,[1,63] N. Cao,[1,63] S. A. Cetin,[62a] J. F. Chang,[1,58] T. T. Chang,[77] W. L. Chang,[1,63] G. R. Che,[44] G. Chelkov,[37,a] C. Chen,[44] Chao Chen,[55] G. Chen,[1] H. S. Chen,[1,63] M. L. Chen,[1,58,63] S. J. Chen,[43] S. M. Chen,[61] T. Chen,[1,63] X. R. Chen,[32,63] X. T. Chen,[1,63] Y. B. Chen,[1,58] Y. Q. Chen,[35] Z. J. Chen,[26,h] W. S. Cheng,[74c] S. K. Choi,[10] X. Chu,[44] G. Cibinetto,[30a] S. C. Coen,[4] F. Cossio,[74c] J. J. Cui,[50] H. L. Dai,[1,58] J. P. Dai,[79] A. Dbeyssi,[19] R. E. de Boer,[4] D. Dedovich,[37] Z. Y. Deng,[1] A. Denig,[36] I. Denysenko,[37] M. Destefanis,[74a,74c] F. De Mori,[74a,74c] B. Ding,[66,1] X. X. Ding,[47,g] Y. Ding,[35] Y. Ding,[41] J. Dong,[1,58] L. Y. Dong,[1,63] M. Y. Dong,[1,58,63] X. Dong,[76] S. X. Du,[81] Z. H. Duan,[43] P. Egorov,[37,a] Y. L. Fan,[76] J. Fang,[1,58] S. S. Fang,[1,63] W. X. Fang,[1] Y. Fang,[1] R. Farinelli,[30a] L. Fava,[74b,74c] F. Feldbauer,[4] G. Felici,[29a] C. Q. Feng,[71,58] J. H. Feng,[59] K. Fischer,[69] M. Fritsch,[4] C. Fritzsch,[68] C. D. Fu,[1] J. L. Fu,[63] Y. W. Fu,[1] H. Gao,[63] Y. N. Gao,[47,g] Yang Gao,[71,58] S. Garbolino,[74c] I. Garzia,[30a,30b] P. T. Ge,[76] Z. W. Ge,[43] C. Geng,[59] E. M. Gersabeck,[67] A. Gilman,[69] K. Goetzen,[14] L. Gong,[41] W. X. Gong,[1,58] W. Gradl,[36] S. Gramigna,[30a,30b] M. Greco,[74a,74c] M. H. Gu,[1,58] Y. T. Gu,[16] C. Y. Guan,[1,63] Z. L. Guan,[23] A. Q. Guo,[32,63] L. B. Guo,[42] M. J. Guo,[50] R. P. Guo,[49] Y. P. Guo,[12,f] A. Guskov,[37,a] X. T. Hou,[1,63] T. T. Han,[50] W. Y. Han,[40] X. Q. Hao,[20] F. A. Harris,[65] K. K. He,[55] K. L. He,[1,63] F. H. H. Heinsius,[4] C. H. Heinz,[36] Y. K. Heng,[1,58,63] C. Herold,[60] T. Holtmann,[4] P. C. Hong,[12,f] G. Y. Hou,[1,63] Y. R. Hou,[63] Z. L. Hou,[1] H. M. Hu,[1,63] J. F. Hu,[56,i] T. Hu,[1,58,63] Y. Hu,[1] G. S. Huang,[71,58] K. X. Huang,[59] L. Q. Huang,[32,63] X. T. Huang,[50] Y. P. Huang,[1] T. Hussain,[73] N. Hüsken,[28,36] W. Imoehl,[28] M. Irshad,[71,58] J. Jackson,[28] S. Jaeger,[4] S. Janchiv,[33] J. H. Jeong,[10] Q. Ji,[1] Q. P. Ji,[20] X. B. Ji,[1,63] X. L. Ji,[1,58] Y. Y. Ji,[50] X. Q. Jia,[50] Z. K. Jia,[71,58] P. C. Jiang,[47,g] S. S. Jiang,[40] T. J. Jiang,[17] X. S. Jiang,[1,58,63] Y. Jiang,[63] J. B. Jiao,[50] Z. Jiao,[24] S. Jin,[43] Y. Jin,[66] M. Q. Jing,[1,63] T. Johansson,[75] X. Kui,[1] S. Kabana,[34] N. Kalantar-Nayestanaki,[64] X. L. Kang,[9] X. S. Kang,[41] R. Kappert,[64] M. Kavatsyuk,[64] B. C. Ke,[81] A. Khoukaz,[68] R. Kiuchi,[1] R. Kliemt,[14] L. Koch,[38] O. B. Kolcu,[62a] B. Kopf,[4] M. K. Kuessner,[4] A. Kupsc,[45,75] W. Kühn,[38] J. J. Lane,[67] J. S. Lange,[38] P. Larin,[19] A. Lavania,[27] L. Lavezzi,[74a,74c] T. T. Lei,[71,k] Z. H. Lei,[71,58] H. Leithoff,[36] M. Lellmann,[36] T. Lenz,[36] C. Li,[48] C. Li,[44] C. H. Li,[40] Cheng Li,[71,58] D. M. Li,[81] F. Li,[1,58] G. Li,[1] H. Li,[71,58] H. B. Li,[1,63] H. J. Li,[20] H. N. Li,[56,i] Hui Li,[44] J. R. Li,[61] J. S. Li,[59] J. W. Li,[50] K. L. Li,[20] Ke Li,[1] L. J. Li,[1,63] L. K. Li,[1] Lei Li,[3] M. H. Li,[44] P. R. Li,[39,j,k] Q. X. Li,[50] S. X. Li,[12] T. Li,[50] W. D. Li,[1,63] W. G. Li,[1] X. H. Li,[71,58] X. L. Li,[50] Xiaoyu Li,[1,63] Y. G. Li,[47,g] Z. J. Li,[59] Z. X. Li,[16] C. Liang,[43] H. Liang,[1,63] H. Liang,[71,58] H. Liang,[35] Y. F. Liang,[54] Y. T. Liang,[32,63] G. R. Liao,[15] L. Z. Liao,[50] J. Libby,[27] A. Limphirat,[60] D. X. Lin,[32,63] T. Lin,[1] B. J. Liu,[1] B. X. Liu,[76] C. Liu,[35] C. X. Liu,[1] D. Liu,[19,71] F. H. Liu,[53] Fang Liu,[1] Feng Liu,[6] G. M. Liu,[56,i] H. Liu,[39,j,k] H. B. Liu,[16] H. M. Liu,[1,63] Huanhuan Liu,[1] Huihui Liu,[22] J. B. Liu,[71,58] J. L. Liu,[72] J. Y. Liu,[1,63]

K. Liu,[1] K. Y. Liu,[41] Ke Liu,[23] L. Liu,[71,58] L. C. Liu,[44] Lu Liu,[44] M. H. Liu,[12,f] P. L. Liu,[1] Q. Liu,[63] S. B. Liu,[71,58] T. Liu,[12,f] W. K. Liu,[44] W. M. Liu,[71,58] X. Liu,[39,j,k] Y. Liu,[39,j,k] Y. Liu,[81] Y. B. Liu,[44] Z. A. Liu,[1,58,63] Z. Q. Liu,[50] X. C. Lou,[1,58,63] F. X. Lu,[59] H. J. Lu,[24] J. G. Lu,[1,58] X. L. Lu,[1] Y. Lu,[7] Y. P. Lu,[1,58] Z. H. Lu,[1,63] C. L. Luo,[42] M. X. Luo,[80] T. Luo,[12,f] X. L. Luo,[1,58] X. R. Lyu,[63] Y. F. Lyu,[44] F. C. Ma,[41] H. L. Ma,[1] J. L. Ma,[1,63] L. L. Ma,[50] M. M. Ma,[1,63] Q. M. Ma,[1] R. Q. Ma,[1,63] R. T. Ma,[63] X. Y. Ma,[1,58] Y. Ma,[47,g] Y. M. Ma,[32] F. E. Maas,[19] M. Maggiora,[74a,74c] S. Malde,[69] A. Mangoni,[29b] Y. J. Mao,[47,g] Z. P. Mao,[1] S. Marcello,[74a,74c] Z. X. Meng,[66] J. G. Messchendorp,[14,64] G. Mezzadri,[30a] H. Miao,[1,63] T. J. Min,[43] R. E. Mitchell,[28] X. H. Mo,[1,58,63] N. Yu. Muchnoi,[13,b] Y. Nefedov,[37] F. Nerling,[19,d] I. B. Nikolaev,[13,b] Z. Ning,[1,58] S. Nisar,[11,l] Y. Niu,[50] S. L. Olsen,[63] Q. Ouyang,[1,58,63] S. Pacetti,[29b,29c] X. Pan,[55] Y. Pan,[57] A. Pathak,[35] P. Patteri,[29a] Y. P. Pei,[71,58] M. Pelizaeus,[4] H. P. Peng,[71,58] K. Peters,[14,d] J. L. Ping,[42] R. G. Ping,[1,63] S. Plura,[36] S. Pogodin,[37] V. Prasad,[34] F. Z. Qi,[1] H. Qi,[71,58] H. R. Qi,[61] M. Qi,[43] T. Y. Qi,[12,f] S. Qian,[1,58] W. B. Qian,[63] C. F. Qiao,[63] J. J. Qin,[72] L. Q. Qin,[15] X. P. Qin,[12,f] X. S. Qin,[50] Z. H. Qin,[1,58] J. F. Qiu,[1] S. Q. Qu,[61] C. F. Redmer,[36] K. J. Ren,[40] A. Rivetti,[74c] V. Rodin,[64] M. Rolo,[74c] G. Rong,[1,63] Ch. Rosner,[19] S. N. Ruan,[44] N. Salone,[45] A. Sarantsev,[37,c] Y. Schelhaas,[36] K. Schoenning,[75] M. Scodeggio,[30a,30b] K. Y. Shan,[12,f] W. Shan,[25] X. Y. Shan,[71,58] J. F. Shangguan,[55] L. G. Shao,[1,63] M. Shao,[71,58] C. P. Shen,[12,f] H. F. Shen,[1,63] W. H. Shen,[63] X. Y. Shen,[1,63] B. A. Shi,[63] H. C. Shi,[71,58] J. L. Shi,[12] J. Y. Shi,[1] Q. Q. Shi,[55] R. S. Shi,[1,63] X. Shi,[1,58] J. J. Song,[20] T. Z. Song,[59] W. M. Song,[35,1] Y. J. Song,[12] Y. X. Song,[47,g] S. Sosio,[74a,74c] S. Spataro,[74a,74c] F. Stieler,[36] Y. J. Su,[63] G. B. Sun,[76] G. X. Sun,[1] H. Sun,[63] H. K. Sun,[1] J. F. Sun,[20] K. Sun,[61] L. Sun,[76] S. S. Sun,[1,63] T. Sun,[1,63] W. Y. Sun,[35] Y. Sun,[9] Y. J. Sun,[71,58] Y. Z. Sun,[1] Z. T. Sun,[50] Y. X. Tan,[71,58] C. J. Tang,[54] G. Y. Tang,[1] J. Tang,[59] Y. A. Tang,[76] L. Y. Tao,[72] Q. T. Tao,[26,h] M. Tat,[69] J. X. Teng,[71,58] V. Thoren,[75] W. H. Tian,[59] W. H. Tian,[52] Y. Tian,[32,63] Z. F. Tian,[76] I. Uman,[62b] S. J. Wang,[50] B. Wang,[1] B. L. Wang,[63] Bo Wang,[71,58] C. W. Wang,[43] D. Y. Wang,[47,g] F. Wang,[72] H. J. Wang,[39,j,k] H. P. Wang,[1,63] J. P. Wang,[50] K. Wang,[1,58] L. L. Wang,[1] M. Wang,[50] Meng Wang,[1,63] S. Wang,[12,f] S. Wang,[39,j,k] T. Wang,[12,f] T. J. Wang,[44] W. Wang,[72] W. Wang,[59] W. P. Wang,[71,58] X. Wang,[47,g] X. F. Wang,[39,j,k] X. J. Wang,[40] X. L. Wang,[12,f] Y. Wang,[61] Y. D. Wang,[46] Y. F. Wang,[1,58,63] Y. H. Wang,[48] Y. N. Wang,[46] Y. Q. Wang,[1] Yaqian Wang,[18,1] Yi Wang,[61] Z. Wang,[1,58] Z. L. Wang,[72] Z. Y. Wang,[1,63] Ziyi Wang,[63] D. Wei,[70] D. H. Wei,[15] F. Weidner,[68] S. P. Wen,[1] C. W. Wenzel,[4] U. W. Wiedner,[4] G. Wilkinson,[69] M. Wolke,[75] L. Wollenberg,[4] C. Wu,[40] J. F. Wu,[1,63] L. H. Wu,[1] L. J. Wu,[1,63] X. Wu,[12,f] X. H. Wu,[35] Y. Wu,[71] Y. J. Wu,[32] Z. Wu,[1,58] L. Xia,[71,58] X. M. Xian,[40] T. Xiang,[47,g] D. Xiao,[39,j,k] G. Y. Xiao,[43] H. Xiao,[12,f] S. Y. Xiao,[1] Y. L. Xiao,[12,f] Z. J. Xiao,[42] C. Xie,[43] X. H. Xie,[47,g] Y. Xie,[50] Y. G. Xie,[1,58] Y. H. Xie,[6] Z. P. Xie,[71,58] T. Y. Xing,[1,63] C. F. Xu,[1,63] C. J. Xu,[59] G. F. Xu,[1] H. Y. Xu,[66] Q. J. Xu,[17] Q. N. Xu,[31] W. Xu,[1,63] W. L. Xu,[66] X. P. Xu,[55] Y. C. Xu,[78] Z. P. Xu,[43] Z. S. Xu,[63] F. Yan,[12,f] L. Yan,[12,f] W. B. Yan,[71,58] W. C. Yan,[81] X. Q. Yan,[1] H. J. Yang,[51,e] H. L. Yang,[35] H. X. Yang,[1] Tao Yang,[1] Y. Yang,[12,f] Y. F. Yang,[44] Y. X. Yang,[1,63] Yifan Yang,[1,63] Z. W. Yang,[39,j,k] Z. P. Yao,[50] M. Ye,[1,58] M. H. Ye,[8] J. H. Yin,[1] Z. Y. You,[59] B. X. Yu,[1,58,63] C. X. Yu,[44] G. Yu,[1,63] J. S. Yu,[26,h] T. Yu,[72] X. D. Yu,[47,g] C. Z. Yuan,[1,63] L. Yuan,[2] S. C. Yuan,[1] X. Q. Yuan,[1] Y. Yuan,[1,63] Z. Y. Yuan,[59] C. X. Yue,[40] A. A. Zafar,[73] F. R. Zeng,[50] X. Zeng,[12,f] Y. Zeng,[26,h] Y. J. Zeng,[1,63] X. Y. Zhai,[35] Y. C. Zhai,[50] Y. H. Zhan,[59] A. Q. Zhang,[1,63] B. L. Zhang,[1,63] B. X. Zhang,[1] D. H. Zhang,[44] G. Y. Zhang,[20] H. Zhang,[71] H. H. Zhang,[35] H. H. Zhang,[59] H. Q. Zhang,[1,58,63] H. Y. Zhang,[1,58] J. J. Zhang,[52] J. L. Zhang,[21] J. Q. Zhang,[42] J. W. Zhang,[1,58,63] J. X. Zhang,[39,j,k] J. Y. Zhang,[1] J. Z. Zhang,[1,63] Jianyu Zhang,[63] Jiawei Zhang,[1,63] L. M. Zhang,[61] L. Q. Zhang,[59] Lei Zhang,[43] P. Zhang,[1] Q. Y. Zhang,[40,81] Shuihan Zhang,[1,63] Shulei Zhang,[26,h] X. D. Zhang,[46] X. M. Zhang,[1] X. Y. Zhang,[50] X. Y. Zhang,[55] Y. Zhang,[69] Y. Zhang,[72] Y. T. Zhang,[81] Y. H. Zhang,[1,58] Yan Zhang,[71,58] Yao Zhang,[1] Z. H. Zhang,[1] Z. L. Zhang,[35] Z. Y. Zhang,[44] Z. Y. Zhang,[76] G. Zhao,[1] J. Zhao,[40] J. Y. Zhao,[1,63] J. Z. Zhao,[1,58] Lei Zhao,[71,58] Ling Zhao,[1] M. G. Zhao,[44] S. J. Zhao,[81] Y. B. Zhao,[1,58] Y. X. Zhao,[32,63] Z. G. Zhao,[71,58] A. Zhemchugov,[37,a] B. Zheng,[72] J. P. Zheng,[1,58] W. J. Zheng,[1,63] Y. H. Zheng,[63] B. Zhong,[42] X. Zhong,[59] H. Zhou,[50] L. P. Zhou,[1,63] X. Zhou,[76] X. K. Zhou,[6] X. R. Zhou,[71,58] X. Y. Zhou,[40] Y. Z. Zhou,[12,f] J. Zhu,[44] K. Zhu,[1] K. J. Zhu,[1,58,63] L. Zhu,[35] L. X. Zhu,[63] S. H. Zhu,[70] S. Q. Zhu,[43] T. J. Zhu,[12,f] W. J. Zhu,[12,f] Y. C. Zhu,[71,58] Z. A. Zhu,[1,63] J. H. Zou,[1] and J. Zu[71,58]

(BESIII Collaboration)

[1]*Institute of High Energy Physics, Beijing 100049, People's Republic of China*
[2]*Beihang University, Beijing 100191, People's Republic of China*
[3]*Beijing Institute of Petrochemical Technology, Beijing 102617, People's Republic of China*
[4]*Bochum Ruhr-University, D-44780 Bochum, Germany*
[5]*Carnegie Mellon University, Pittsburgh, Pennsylvania 15213, USA*

[6]Central China Normal University, Wuhan 430079, People's Republic of China
[7]Central South University, Changsha 410083, People's Republic of China
[8]China Center of Advanced Science and Technology, Beijing 100190, People's Republic of China
[9]China University of Geosciences, Wuhan 430074, People's Republic of China
[10]Chung-Ang University, Seoul, 06974, Republic of Korea
[11]COMSATS University Islamabad, Lahore Campus, Defence Road, Off Raiwind Road, 54000 Lahore, Pakistan
[12]Fudan University, Shanghai 200433, People's Republic of China
[13]G.I. Budker Institute of Nuclear Physics SB RAS (BINP), Novosibirsk 630090, Russia
[14]GSI Helmholtzcentre for Heavy Ion Research GmbH, D-64291 Darmstadt, Germany
[15]Guangxi Normal University, Guilin 541004, People's Republic of China
[16]Guangxi University, Nanning 530004, People's Republic of China
[17]Hangzhou Normal University, Hangzhou 310036, People's Republic of China
[18]Hebei University, Baoding 071002, People's Republic of China
[19]Helmholtz Institute Mainz, Staudinger Weg 18, D-55099 Mainz, Germany
[20]Henan Normal University, Xinxiang 453007, People's Republic of China
[21]Henan University, Kaifeng 475004, People's Republic of China
[22]Henan University of Science and Technology, Luoyang 471003, People's Republic of China
[23]Henan University of Technology, Zhengzhou 450001, People's Republic of China
[24]Huangshan College, Huangshan 245000, People's Republic of China
[25]Hunan Normal University, Changsha 410081, People's Republic of China
[26]Hunan University, Changsha 410082, People's Republic of China
[27]Indian Institute of Technology Madras, Chennai 600036, India
[28]Indiana University, Bloomington, Indiana 47405, USA
[29a]INFN Laboratori Nazionali di Frascati, I-00044, Frascati, Italy
[29b]INFN Sezione di Perugia, I-06100, Perugia, Italy
[29c]University of Perugia, I-06100, Perugia, Italy
[30a]INFN Sezione di Ferrara, I-44122, Ferrara, Italy
[30b]University of Ferrara, I-44122, Ferrara, Italy
[31]Inner Mongolia University, Hohhot 010021, People's Republic of China
[32]Institute of Modern Physics, Lanzhou 730000, People's Republic of China
[33]Institute of Physics and Technology, Peace Avenue 54B, Ulaanbaatar 13330, Mongolia
[34]Instituto de Alta Investigación, Universidad de Tarapacá, Casilla 7D, Arica, Chile
[35]Jilin University, Changchun 130012, People's Republic of China
[36]Johannes Gutenberg University of Mainz, Johann-Joachim-Becher-Weg 45, D-55099 Mainz, Germany
[37]Joint Institute for Nuclear Research, 141980 Dubna, Moscow region, Russia
[38]Justus-Liebig-Universitaet Giessen, II. Physikalisches Institut, Heinrich-Buff-Ring 16, D-35392 Giessen, Germany
[39]Lanzhou University, Lanzhou 730000, People's Republic of China
[40]Liaoning Normal University, Dalian 116029, People's Republic of China
[41]Liaoning University, Shenyang 110036, People's Republic of China
[42]Nanjing Normal University, Nanjing 210023, People's Republic of China
[43]Nanjing University, Nanjing 210093, People's Republic of China
[44]Nankai University, Tianjin 300071, People's Republic of China
[45]National Centre for Nuclear Research, Warsaw 02-093, Poland
[46]North China Electric Power University, Beijing 102206, People's Republic of China
[47]Peking University, Beijing 100871, People's Republic of China
[48]Qufu Normal University, Qufu 273165, People's Republic of China
[49]Shandong Normal University, Jinan 250014, People's Republic of China
[50]Shandong University, Jinan 250100, People's Republic of China
[51]Shanghai Jiao Tong University, Shanghai 200240, People's Republic of China
[52]Shanxi Normal University, Linfen 041004, People's Republic of China
[53]Shanxi University, Taiyuan 030006, People's Republic of China
[54]Sichuan University, Chengdu 610064, People's Republic of China
[55]Soochow University, Suzhou 215006, People's Republic of China
[56]South China Normal University, Guangzhou 510006, People's Republic of China
[57]Southeast University, Nanjing 211100, People's Republic of China
[58]State Key Laboratory of Particle Detection and Electronics, Beijing 100049, Hefei 230026, People's Republic of China
[59]Sun Yat-Sen University, Guangzhou 510275, People's Republic of China

[60]*Suranaree University of Technology, University Avenue 111, Nakhon Ratchasima 30000, Thailand*
[61]*Tsinghua University, Beijing 100084, People's Republic of China*
[62a]*Turkish Accelerator Center Particle Factory Group, Istinye University, 34010, Istanbul, Turkey*
[62b]*Near East University, Nicosia, North Cyprus, 99138, Mersin 10, Turkey*
[63]*University of Chinese Academy of Sciences, Beijing 100049, People's Republic of China*
[64]*University of Groningen, NL-9747 AA Groningen, The Netherlands*
[65]*University of Hawaii, Honolulu, Hawaii 96822, USA*
[66]*University of Jinan, Jinan 250022, People's Republic of China*
[67]*University of Manchester, Oxford Road, Manchester, M13 9PL, United Kingdom*
[68]*University of Muenster, Wilhelm-Klemm-Strasse 9, 48149 Muenster, Germany*
[69]*University of Oxford, Keble Road, Oxford OX13RH, United Kingdom*
[70]*University of Science and Technology Liaoning, Anshan 114051, People's Republic of China*
[71]*University of Science and Technology of China, Hefei 230026, People's Republic of China*
[72]*University of South China, Hengyang 421001, People's Republic of China*
[73]*University of the Punjab, Lahore-54590, Pakistan*
[74a]*University of Turin, I-10125, Turin, Italy*
[74b]*University of Eastern Piedmont, I-15121, Alessandria, Italy*
[74c]*INFN, I-10125, Turin, Italy*
[75]*Uppsala University, Box 516, SE-75120 Uppsala, Sweden*
[76]*Wuhan University, Wuhan 430072, People's Republic of China*
[77]*Xinyang Normal University, Xinyang 464000, People's Republic of China*
[78]*Yantai University, Yantai 264005, People's Republic of China*
[79]*Yunnan University, Kunming 650500, People's Republic of China*
[80]*Zhejiang University, Hangzhou 310027, People's Republic of China*
[81]*Zhengzhou University, Zhengzhou 450001, People's Republic of China*

[a]Also at the Moscow Institute of Physics and Technology, Moscow 141700, Russia.
[b]Also at the Novosibirsk State University, Novosibirsk, 630090, Russia.
[c]Also at the NRC "Kurchatov Institute", PNPI, 188300, Gatchina, Russia.
[d]Also at Goethe University Frankfurt, 60323 Frankfurt am Main, Germany.
[e]Also at Key Laboratory for Particle Physics, Astrophysics and Cosmology, Ministry of Education; Shanghai Key Laboratory for Particle Physics and Cosmology; Institute of Nuclear and Particle Physics, Shanghai 200240, People's Republic of China.
[f]Also at Key Laboratory of Nuclear Physics and Ion-beam Application (MOE) and Institute of Modern Physics, Fudan University, Shanghai 200443, People's Republic of China.
[g]Also at State Key Laboratory of Nuclear Physics and Technology, Peking University, Beijing 100871, People's Republic of China.
[h]Also at School of Physics and Electronics, Hunan University, Changsha 410082, China.
[i]Also at Guangdong Provincial Key Laboratory of Nuclear Science, Institute of Quantum Matter, South China Normal University, Guangzhou 510006, China.
[j]Also at Frontiers Science Center for Rare Isotopes, Lanzhou University, Lanzhou 730000, People's Republic of China.
[k]Also at Lanzhou Center for Theoretical Physics, Lanzhou University, Lanzhou 730000, People's Republic of China.
[l]Also at the Department of Mathematical Sciences, IBA, Karachi 75270, Pakistan.